Letter

Precursors of the El Niño phenomenon: A climate network analysis

Rupali Sonone[1,*] and Neelima Gupte[2,†]
[1]*Department of Physics, Indian Institute of Technology Madras, Chennai 600036, India*
[2]*Department of Physics, Indian Institute of Technology Madras, Chennai 600036, India*
and Complex Systems and Dynamics Group, Indian Institute of Technology Madras, Chennai 600036, India

(Received 18 October 2019; accepted 23 March 2021; published 16 April 2021)

The identification of precursors of climatic phenomena has enormous practical importance. Recent work constructs a climate network based on surface air temperature data to analyze the El Niño phenomena. We utilize microtransitions which occur before the discontinuous percolation transition in the network as well as other network quantities to identify a set of reliable precursors of El Niño episodes. These precursors identify 10 out of 13 El Niño episodes occurring in the period of 1979–2018 with an average lead time of approximately 6.4 months. We also find indicators of tipping events in the data.

DOI: 10.1103/PhysRevE.103.L040301

I. INTRODUCTION

The climate system is a highly complex nonlinear dynamical system consisting of various subsystems such as the atmosphere, the ocean, the cryosphere, etc. The nonlinear interactions within these subsystems lead to climatic phenomena on multiple timescales such as cyclones, monsoons, and oceanic currents [1]. These phenomena have major consequences for ecological and economic events. Hence the prediction of such events has practical utility, but is difficult to achieve due to their complex nature. Therefore, the construction of reliable predictors of such events is useful and important. Recent methods proposed to analyze such systems include the construction of complex networks from climate data [1–3] which have been used to forecast important phenomena, e.g., monsoons [4,5], the North Atlantic Oscillation, and El Niño events [6–12].

These networks are constructed using massive datasets consisting of the time series of weather observations at different geographic locations. These locations are chosen to be nodes, and links are added between nodes based on correlations between the dynamics. Recently, the utility of designing generic tools that reliably track the structural changes in the network has been highlighted [12]. Tracking these structural changes in these networks reveals severe responses to climatic events such as El Niño events.

The El Niño Southern Oscillation (ENSO) discussed here is the most influential climate phenomenon on interannual timescales, and is marked by irregular warm (El Niño) and cold (La Niña) anomalies of sea surface temperatures (SSTs) from the long-term mean state. Events are defined as the consecutive overlapping of 3-month periods of SST anomalies ($\geqslant +0.5\,^{\circ}$C) for warm (El Niño) events and ($\leqslant -0.5\,^{\circ}$C) for cold (La Niña) events in the Niño 3.4 region (i.e., 5° N-5° S, 120°–170° W). The threshold is further broken down into weak (0.5 °C–0.9 °C SST anomaly), moderate (1.0 °C–1.4 °C), strong (1.5 °C–1.9 °C), and very strong ($\geqslant 2.0\,^{\circ}$C) events. This phenomenon triggers many disruptions around the globe causing disastrous flooding or severe droughts in large areas of South America, Asia, and Australia, severe winters in Europe, intense tropical cyclones in the Caribbean, and epidemic diseases occurring in various places [13,14]. The ENSO phenomenon is currently quantified by the NINO 3.4 index. Here, the datasets of the near surface air temperature of ERA-Interim reanalysis [The European Centre for Medium-Range Weather Forecasts (ECMWF)] within the period 1979–2018 are used to forecast the development of the El Niño well in advance [15]. Early forecasts of the El Niño event can contribute to better disaster management and efficient distribution of resources well before the calamity.

Complex networks which represent a wide range of systems, e.g., ecosystems, financial markets, and the climate, can have tipping points at which a phase transition to a contrasting dynamical regime occurs. A variety of indicators, such as the order parameter and the susceptibility, quantify the loss of resilience which occurs when the systems approach the transition point [16,17]. Percolation theory and the behavior of connected clusters has been used to predict the transition point [18] for climate networks, where discontinuous transitions with associated jumps in the order parameter have been observed. We analyze these discontinuous transitions and identify a set of early warning precursors to these transitions, and use them to predict the onset of El Niño activity about 4–10 months in advance. Our methods are quite reliable, and only lead to a single missed prediction in the analysis of 40 years of data, and include the analysis of microtransitions, and the identification of topological network quantities such as node degrees, link densities, and link lengths.

In the context of percolation, microtransitions are small jumps in the order parameter, i.e., the size of the maximal

*vaidehisonone@gmail.com
†gupte@physics.iitm.ac.in

cluster, which occur before the transition to percolation, and accumulate at the transition point [19]. These microtransitions are signaled by peaks in the variance of the order parameter, and can be used to predict critical thresholds at which the percolation transition occurs. For climate networks, these values are characteristic of the data of the period for which the network is constructed and can hence be used as generic early-warning indicators of the El Niño years. The variance in the order parameter, i.e., the susceptibility at the critical point, can also be used to identify pre–El Niño years (indicator years), and predict El Niño events in the subsequent year. We note that the jump in the order parameter has been used earlier to identify pre–El Niño years [20], but the susceptibility constitutes a stronger indicator. Additionally, we have carried out the topological analysis of the climate network of each year and have found that several distinct features such as the number of links and the degrees of the nodes in the El Niño basin, differentiate clearly between El Niño years and indicator years. Thus, this entire collection of features, i.e., the susceptibility, the total number of links, the node degree (the degree of the most linked node), the maximum value of correlation strength, and the critical correlation value observed for the climate network can be used as a set of precursors to an upcoming El Niño event.

II. THE CONSTRUCTION OF THE NETWORK

The climate network is constructed by using daily near surface (1000 hPa, nearly equal to one atmospheric pressure) air temperature datasets $[\tilde{T}^y(d)]$ recorded at 115,680 nodes whose geographical locations are fixed by latitude and longitude values. The grid size of the network can be altered by changing the resolution of nodes such that every element in the grid covers the same area on the globe. The available datasets of the daily near surface (1000 hPa) air temperature of ERA-Interim reanalysis (ECMWF) have 115,680 total number of grid points (nodes) with 0.75° grid resolution out of which we have extracted data for 726 grid points with 7.5° grid resolution that approximately homogeneously cover the entire globe. Thus the total number of nodes on the equator is given by $n_0 = 360^\circ/r_0$, where r_0 is the grid resolution, and the total number of nodes on mr_0 latitude is given by $n_m = n_0 \cos(mr_0)$ where $m \in [-90/r_0, 90/r_0]$. The total number of nodes in the climate network is then $N = \sum_{m=0}^{m=90/r_0} 2n_m - n_0$. A geographical grid of 726 nodes with a grid resolution of 7.5° is constructed. Links are added between two nodes by calculating the Pearson correlation function between their temperatures. The filtered daily near surface air temperature $T^y(d)$ and the cross-correlation function $C^y_{i,j}$ are defined by [20]

$$T^y(d) = \frac{\tilde{T}^y(d) - \text{mean}[\tilde{T}(d)]}{\text{std}[\tilde{T}(d)]}, \tag{1}$$

$$C^y_{i,j}(\tau) = \frac{\langle T^y_i(d-\tau)T^y_j(d)\rangle - \langle T^y_i(d-\tau)\rangle\langle T^y_j(d)\rangle}{\sqrt{\left[T^y_i(d-\tau) - \langle T^y_i(d-\tau)\rangle\right]^2}.\sqrt{\left[T^y_j(d) - \langle T^y_j(d)\rangle\right]^2}}. \tag{2}$$

Temperature datasets for 40 years from 1979 to 2018 have been used to build a network for each year from January 1st to December 31st. Here, τ is the time lag ranging from 0 to 200 days where the choice of time lag is discussed in [21] and temperature data points prior to day "d" are considered for the lagged data. Here, the quantities "mean" and "std" are the mean and standard deviation of the temperature on day "d" over all years and the averages ($\langle\cdot\rangle_d$) are taken over 365 days. The weight of the link between i and j is defined as the maximum of the cross-correlation function $\max[C^y_{i,j}(\tau)]$. First, the links or edges with the highest weight (the largest value of the cross-correlation function $C^y_{i,j}$) are added to the network and later links are added in order of decreasing link strength. Thus the network evolves as a function of C, as links of weights ranging from a given value of C up to the maximum value of C (which is $C_{\max}$) are added at each stage. $C_{\max}$ is the maximum link weight obtained from the correlation. Quantities such as the order parameter, which is the normalized size of the largest cluster (s_1) and the susceptibility (χ) for each distinct value of C, are defined by [20]

$$s_1 = \frac{S_1}{N}, \tag{3}$$

$$\chi = \frac{\sum'_s s^2 n_s(C)}{\sum'_s s n_s(C)}. \tag{4}$$

Here, S_1 is the size of the largest cluster, N is the total number of nodes, $n_s(C)$ is the number of clusters of size "s" for link's weight C and below, and the prime on the sums indicates the exclusion of the largest cluster S_1 in each measurement. The transition to the percolating state in this climate network is identified via the existence of a giant cluster containing $O(N)$ nodes. Precursors which can predict this transition can prove to be highly useful in the prediction of the El Niño and other climatic phenomena.

III. PRECURSORS AND INDICATORS OF THE TRANSITION

We note that El Niño events have been classified as very strong, strong, and moderate events based on the El Niño index, and compare the networks corresponding to each class. These networks are characterized by plotting the susceptibility (χ) and the largest normalized cluster (s_1). We plot these quantities as functions of C for typical years with El Niño events of each class, as well as the preceding years, which turn out to be indicator years of the event (see Fig. 1).

The year is indicated at the top of all the plots, and the red line marks the critical value C_c on the x axis at which the largest jump is observed in s_1. The transition to percolation is signaled by the value of s_1 tending toward 1, and the existence of a maximal cluster. A discontinuous phase transition

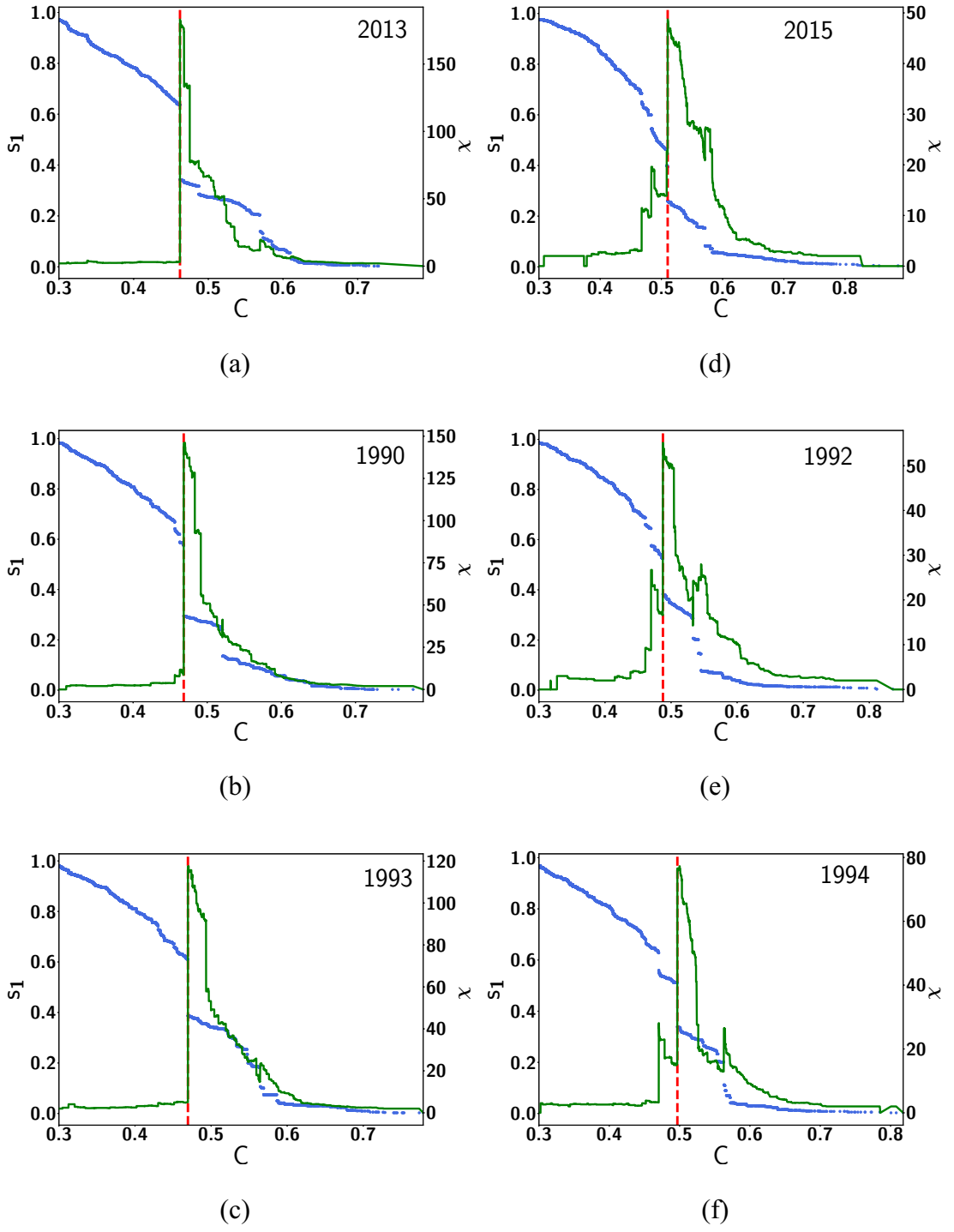

FIG. 1. The largest cluster s_1 (blue dotted line) and susceptibility χ (green line) is plotted as a function of the link strength C for the network. Plots (a) December 2013, (b) December 1990, and (c) December 1993, which are years which precede a very strong El Niño episode, strong El Niño episode, and a moderate El Niño episode, respectively. Plots (d)–(f) are for years when the El Niño episode peaks: (d) very strong El Niño episode, December 2015; (e) strong El Niño episode, December 1992; (f) moderate El Niño episode, December 1994.

is clearly seen in s_1 and the jump in the size of the maximal cluster Δs_1 is the largest for the indicator year, i.e., 1 year prior to the El Niño episode. The susceptibility χ is also plotted on the same graphs. It can be seen that the magnitude of the jump $\Delta\chi$ is significantly larger in the indicator years compared to other years.

The susceptibility of the network gives a measure of the variation in the spread of clusters of different sizes at a given correlation strength. We note that while the jump in the order parameter has been suggested as a precursor [20], the susceptibility constitutes a more definitive and reliable precursor for the upcoming El Niño episode as not only is the largest

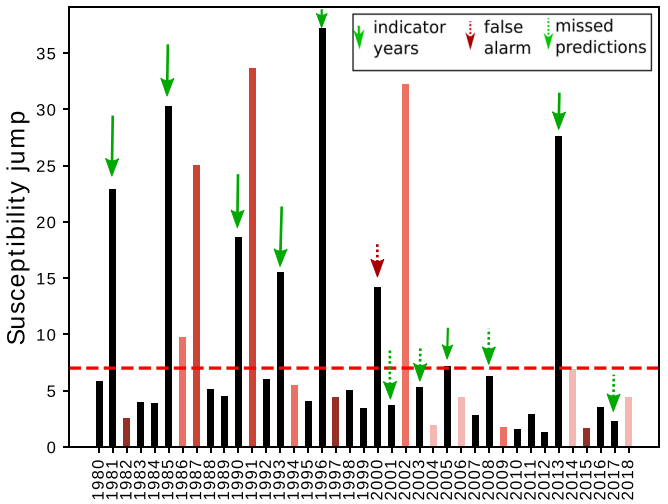

FIG. 2. The maximum jump in the susceptibility χ for each year (1979–2018). El Niño years are shown in red with a gradation according to their strength. There have been 13 such El Niño episodes out of which 1982, 1997, and 2015 are very strong El Niño years; 1987 and 1991 are strong El Niño years; 1986, 1994, 2002, and 2009 are moderate El Niño years; and 2004, 2006, 2014, and 2018 are weak El Niño years. A false alarm (in the year 2000) and the missed predictions (in the years 2001, 2003, 2008, and 2017) are solely based on susceptibility. Note that after taking into account other precursors (as summarized in Table I) we get one false alarm and one missed prediction (in the year 2003).

jump $\Delta\chi$ significant, but the sequence of peaks seen before this jump also has a very distinctive pattern. Reference [20] suggested that the susceptibility did not appear to have a clear relation with the El Niño Index and hence did not use it as a predictor. In contrast to their observations, we show that the susceptibility can be used as a predictor, and also shows a series of small transitions, i.e., microtransitions before the percolation transition point. These quantities can be made to make two distinct predictions. Here, the value of the jump in the susceptibility (Fig. 2) can be used as a precursor of the El Niño event, and the pattern of microtransitions can be used to predict the value C_c at which the percolation transition occurs.

We adopt the following criterion for the prediction of the El Niño. When the maximum jump in the susceptibility crosses a threshold value (here, 7), an El Niño episode is predicted in the following year. This threshold succeeds in the prediction of 7 events correctly out of 13 with just one false alarm. All very strong, strong, and moderate events mentioned here are predicted by our criterion, and only one very weak El Niño event is missed. The threshold has been set to be the value of the jump of the year 2005, which is the indicator year for a weak El Niño year. This minimizes the false alarms.

This should be compared with the results of Ref. [20] where the normalized largest cluster Δs_1 crossing a threshold value (0.286), predicts an El Niño episode in the next year, resulting in seven events being predicted correctly out of ten, with one false alarm between 1980 and 2016.

The susceptibility pattern prior to an El Niño episode is further analyzed by looking at the microtransitions signaled by small jumps in the susceptibility occurring before the phase transition signaled by the largest jump. The scaling relation for the quantity $(C_c - C_{i+1}/C_c - C_i)$ plotted as a function of the index i, the index of the peaks in the susceptibility $\Delta\chi$, can be used to predict the critical value of C_c in the given year as follows.

A. Microtransitions and scaling

Here, C_c is the value of the link strength at which the climate network undergoes the percolation transition, i.e., the formation of a giant component (cluster) containing $O(N)$ nodes [Fig. 3 (inset)]. Figure 3(a) plots the magnitude of successive jumps in the susceptibility with respect to the link strength. Index i defines the ith jump in susceptibility starting from $C_{\max}$. Using the scaling relation of Fig. 3(b) we have

$$\frac{C_c - C_{i+1}}{C_c - C_i} = 0.9956. \tag{5}$$

This scaling relation can be used to predict the critical value C_c for the percolation transition, for the microtransitions in the network for each year. For the indicator year 2014, we find that $C_c = 0.4669$ using the values $i = 44$, $C_{44} = 0.6719$, and $C_{45} = 0.6710$. This value of C_c from the scaling relation is in reasonable agreement with the actual value of $C_c = 0.4522$ obtained from the order parameter jump. A similar pattern of activity is observed for all the pre–El Niño years. We notice that the C_c value ranges from 0.4411 to 0.4736 for all indicator years except for the year 2008 prior to a moderate El Niño episode.

The structure of the network can be analyzed further using topological quantities such as the distribution of the link lengths, the total number of long length links, and the degrees of the nodes. The values of these quantities can also be used for the prediction of El Niño events.

B. Topological analysis of the network

The topological analysis of all 40 climate networks constructed out of the available data has also been carried out. A significant quantity here is the length of the links, $\ell_{i,j}$, i.e., the geographical distance between point i and point j, typically of the order of thousands of kilometers. These remote connections, called teleconnections [12], are of great importance as they reflect the underlying climatic currents mirroring the transportation of energy (Figs. 4 and 5). The total number of teleconnections, the number of long distance links, as well as the number of links with high correlation strengths increase during El Niño episodes, as do nodes of high degree (number of links per node). Figures 5(a) and 5(b) indicate the geographical distribution of nodes of high degree.

It is noticed that the number of large distance links or teleconnections increases significantly during El Niño as well as La Niña activity. See Figs. 4(a), 4(b), 5(c), and 5(d).

The figures above further support the observation that the total number of teleconnections increases significantly during El Niño as well as La Niña activity. An increased number of teleconnections with higher values of correlation strength are also seen for El Niño years. The degrees of nodes (number of links per node) at each grid location have been plotted in Fig. 5(c), and confirm this observation. It can be clearly seen that during very strong El Niño activity, nodes from the

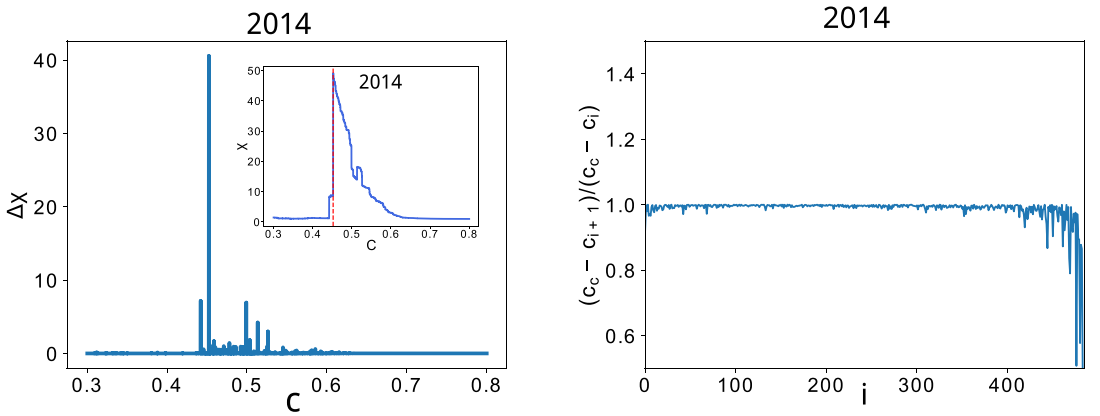

FIG. 3. (a) The jump $\Delta\chi$ as a function of the link strength C. Inset: The susceptibility χ as a function of the link strength C for the network 1 year before a very strong El Niño episode, December 2014. (b) The scaling relation for the relative $\Delta\chi$ positions $(C_c - C_{i+1}/C_c - C_i)$ as a function of the index i.

El Niño basin have higher degree ($\geqslant 40$) and are strongly connected, whereas for indicator years, the degrees of these nodes have a lower value in the range 0–15 and highly connected nodes appear outside the El Niño basin. We thus have a set of topological signatures for the indicator years of the El Niño episodes in addition to the susceptibility, C_c and $C_{\max}$.

IV. CONCLUSIONS

Complete set of characterizers and lead times for prediction

Table I summarizes all the distinct and significant indicators, for indicator years, as well as all the El Niño episodes which occurred between the years 1979 and 2018. The episode durations vary from 5 months to 19 months. The values of the quantity $\Delta\chi$ are significantly higher in indicator years. We see that when the quantity $\Delta\chi$ crosses a threshold value 7, it serves as a predictor of the occurrence of an El Niño event in the subsequent year. Here, a network is constructed for each year using the data of $\approx$565 days and a prediction is made at the end of every year (31st December). We note that if an El Niño episode has already started before this, and continues into the next year, this is not predicted afresh for the next year, e.g., we treat the 18-month episode of 1986-1987-1988, and the 19-month episode of 2014-2016 as single episodes in Table I.

From the data in Table I, the lead time between the prediction and the beginning of the El Niño episodes is $\approx$6.4 months, and is $\approx$11.4 months before the episode peak, when averaged over all the years. Again, the magnitude of $\Delta\chi$ is distinctly higher for indicator years followed by strong and very strong El Niño episodes compared to those followed by weak or moderate episodes. The value C_c at which the network undergoes a discontinuous percolation transition is listed in Table I. Here, the difference between indicator years and El Niño years can be clearly seen. The degrees of the nodes in these years also take high values, as can be seen in

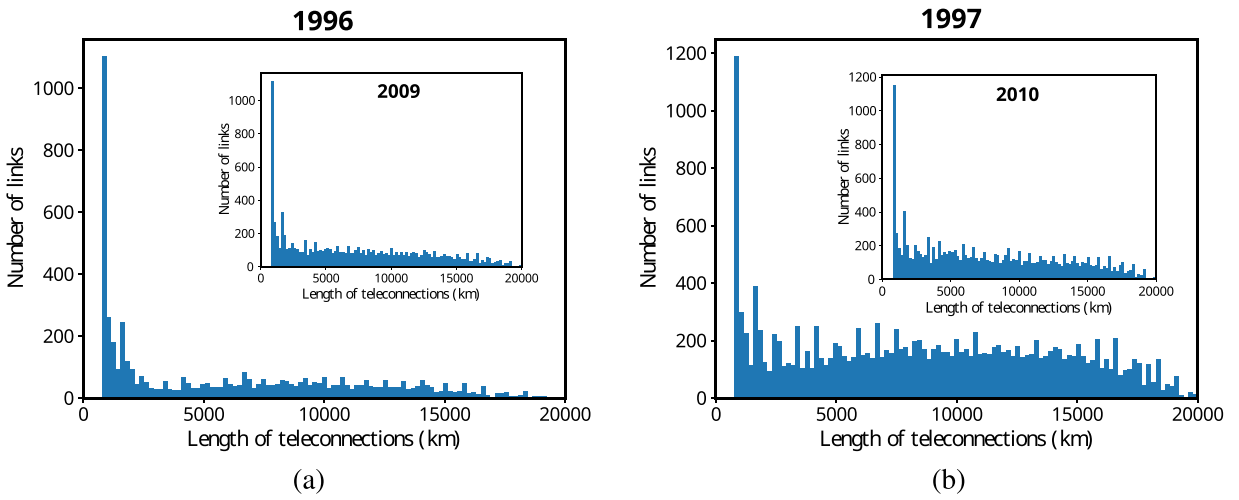

FIG. 4. The histogram of the teleconnections in kilometers for the network. (a) One year before a very strong El Niño episode, December 1996. Inset: One year before strong La Niña episode, December 2009. (b) During a very strong El Niño episode, December 1997. Inset: During a strong La Niña episode, December 2010.

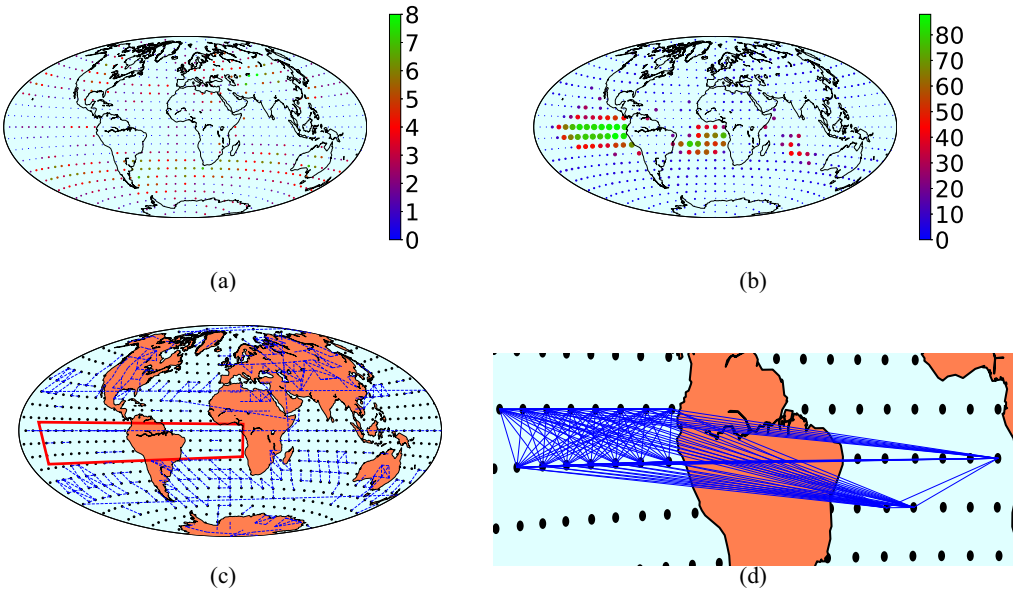

FIG. 5. (i) The geographic distribution of degrees for the nodes of the network for $C = 0.5$ and above. (a) One year before a very strong El Niño episode, December 1996. (b) During a very strong El Niño episode, December 1997. (ii) The teleconnection plots of the networks at $C = 0.5$ and above. (c) One year before a very strong El Niño episode, December 1996. The same quantity in the red rectangular region in (c) is shown during a very strong El Niño episode, December 1997 in (d) indicating the teleconnections between the nodes with degree $\geqslant 70$.

Fig. 5(b). Some of these quantities can be used as precursors in conjunction with the susceptibility jumps and C_c values in years where the El Niño phenomena is mild.

Here, we use three crucial predictors, viz., the jump in the susceptibility, the total number of links, and the degree of nodes. The jump in the susceptibility is used as the first predictor (with the threshold value of the jump being set at 7), as in Fig. 2. If this misses a prediction, as in 2001 and 2008, and 2017, we look at the next two characterizers, viz., the total number of links and the degree. If the values for both these exceed their thresholds (here the threshold for the total number of links is 10 000 and that for the degree of the most linked node is 12), we predict an El Niño episode in the next year. Table I also lists $C_{\max}$ and C_c values for the indicator years and El Niño years. Since these values vary in a narrow range, we treat them as additional confirmation of upcoming events as the C_c values range between $0.4411 < C_c < 0.4736$ for all indicator years except 2008 and shift to higher values for the El Niño years. In the case of $C_{\max}$ the range is $0.7609 < C_{\max} < 0.8430$ for indicator years, and

TABLE I. All El Niño events observed between 1979 and 2018 are listed here with their indicator years, and their duration in boldface. The values of the jump in the susceptibility, as well as the topological characterizers, are listed in the table for El Niño years as well as indicator years. Note that in 1986 the El Niño event lasted for 18 months and in 2014 it lasted for 19 months. Figure 2 shows the 1986 event as a moderate El Niño event followed by a strong El Niño episode observed in 1987. Similarly, Fig. 2 shows a weak El Niño event in 2014 followed by a very strong El Niño event in 2015. These consecutive events have been clubbed together in the table, giving 11 events in all.

Year	$\Delta\chi$	Total number of links	Node degrees	$C_{\max}$	C_c	Year	$\Delta\chi$	Total number of links	Node Node degrees	$C_{\max}$	C_c
1. 1981 (15 months)	22	10108	14	0.7609	0.4411	**7. 2003** (8 months)	5	9393	10	0.7984	0.4856
04/1982 to 06/1983	3	24850	40	0.8863	0.5419	07/2004 to 02/2005	7	10000	9	0.7929	0.4660
2. 1985 (18 months)	30	10601	9	0.7960	0.4536	**8. 2005** (5 months)	7	10000	8	0.7929	0.4660
09/1986 to 02/1988	5	20021	70	0.9361	0.4879	09/2006 to 01/2007	2	12830	35	0.8712	0.4948
3. 1990 (14 months)	18	10592	8	0.7912	0.4682	**9. 2008** (9 months)	6	17882	40	0.8346	0.5126
05/1991 to 06/1992	6	16545	25	0.8513	0.4874	07/2009 to 03/2010	1	24397	70	0.8747	0.5119
4. 1993 (7 months)	15	11981	25	0.7787	0.4695	**10. 2013** (19 months)	27	11170	8	0.7877	0.4620
09/1994 to 03/1995	4	14099	25	0.8538	0.4871	11/2014 to 05/2016	3	20301	50	0.8949	0.5022
5. 1996 (13 months)	37	10331	8	0.8430	0.4736	**11. 2017** (10 months)	2	11224	26	0.7840	0.4980
05/1997 to 05/1998	5	27469	85	0.9520	0.5027	2018	4	12919	30	0.8650	0.5001
6. 2001 (9 months)	3	10122	12	0.8157	0.4660						
06/2002 to 02/2003	5	14311	10	0.7986	0.4856						

$0.7929 < C_{\max} < 0.9520$ for El Niño years. However, the ranges are too small to set a reliable threshold.

We note that the complete set is able to identify the moderate El Niño events in the years 2002-2003, 2009-2010, as well as the weak event seen in 2018. Here, although the jumps in the susceptibility miss picking up these events, Table I clearly shows that the total number of links and the highest node degree both successfully pick up these events, according to the thresholds discussed, and the C_c and $C_{\max}$ values lie in the ranges mentioned above, both for the years of the events and the indicator years. Thus, Table I successfully picks up all the events shown except one, viz., 2003. This emphasizes the importance of looking at the characterizers in conjunction with each other.

Conversely, a false-positive alarm is observed in the year 2000 in the 40 climate networks studied, where the susceptibility and C_c predicted an El Niño in the year 2001, which did not occur due to the presence of a prolonged and strong La Niña episode between July 1998 and February 2001 (32 months). The total number of links and the highest degrees of nodes showed moderate values, viz., 11 000 and 16 in the year 2000, consistent with other indicator years. This further emphasizes the requirement of looking at the full set of indicators for the La Niña years, and for years where the two phenomena occur close to each other. Some preliminary work in this respect is in progress [22]. Further work in this direction could include the improvement of prediction times using sliding windows and the identification of tipping points using link densities in focused geographic regions, e.g., in the area of polar jet streams, i.e., slightly below the tropic of Capricorn and the northwest part of Eurasia [23].

We note that we have not divided the data into a learning and validation phase in the present work. However, the set of precursors constructed here are amenable to automation via machine learning. In the future, we hope to work on more extensive data, and analyze the extent to which the method is successful after dividing the data into learning and validation phases.

V. SUMMARY AND DISCUSSION

To summarize, we have identified a set of precursors for the El Niño phenomena, using the construction of climate networks. These include the susceptibility, the value of the critical correlation, the maximum value of the correlation strength, and the total number of links observed in the climate network. The topological characterizers, i.e., the degree distribution and the total number of links, supplement the information available in the order parameter and the susceptibility. These precursors, taken together, constitute signatures of the indicator year which can reliably predict an El Niño event, 4–10 months in advance, and significantly reduce the frequency of false alarms. We hope our methods provide pointers for other investigations in the context of climate networks.

ACKNOWLEDGMENTS

R.S. thanks IIT Madras for support from an Institute postdoctoral fellowship for the period in which this work was done. N.G. thanks DST-DAAD for a DST-DAAD project and IIT Madras for the CoE Project No. SP20210777DRMHRDDIRIIT.

[1] J. Deza, M. Barreiro, and C. Masoller, Eur. Phys. J.: Spec. Top. **222**, 511 (2013).
[2] M. Barreiro, A. C. Marti, and C. Masoller, Chaos **21**, 013101 (2011).
[3] A. A. Tsonis, K. L. Swanson, and P. J. Roebber, Bull. Am. Meteorol. Soc. **87**, 585 (2006).
[4] N. Malik, B. Bookhagen, N. Marwan, and J. Kurths, Clim. Dyn. **39**, 971 (2012).
[5] V. Stolbova, E. Surovyatkina, B. Bookhagen, and J. Kurths, Geophys. Res. Lett. **43**, 3982 (2016).
[6] K. Yamasaki, A. Gozolchiani, and S. Havlin, Phys. Rev. Lett. **100**, 228501 (2008).
[7] A. A. Tsonis and K. L. Swanson, Phys. Rev. Lett. **100**, 228502 (2008).
[8] J. F. Donges, Y. Zou, N. Marvan, and J. Kurths, Eur. Phys. J.: Spec. Top. **174**, 157 (2009).
[9] J. F. Donges, Y. Zou, N. Marvan, and J. Kurths, Europhys. Lett. **87**, 48007 (2009).
[10] A. Gozolchiani, S. Havlin, and K. Yamasaki, Phys. Rev. Lett. **107**, 148501 (2011).
[11] Y. Wang, A. Gozolchiani, Y. Ashkenazy, Y. Berezin, O. Guez, and S. Havlin, Phys. Rev. Lett. **111**, 138501 (2013).
[12] D. Zhou, A. Gozolchiani, Y. Ashkenazy, and S. Havlin, Phys. Rev. Lett. **115**, 268501 (2015).
[13] M. S. Halpert and C. F. Ropelewski, J. Clim. **5**, 577 (1992).
[14] M. Davis, *Late Victorian Holocausts: El Niño Famines and the Making of the Third World* (Verso, London, 2001).
[15] The European Centre for Medium-Range Weather Forecasts (ECMWF) is an independent intergovernmental organization, http://apps.ecmwf.int/datasets/data/interim-full-daily/levtype=pl/.
[16] V. Rodríguez-Méndez, V. Eguíluz, E. Hernández-García, and J. Ramasco, Sci. Rep. **6**, 29552 (2016).
[17] M. Scheffer, J. Bascompte, W. Brock, V. Brovkin, S. Carpenter, V. Dakos, H. Held, E. van Nes, M. Rietkerk, and G. Sugihara, Nature (London) **461**, 08227 (2009).
[18] D. Stauffer and A. Aharony, *Introduction to Percolation Theory* (Taylor & Francis, London, 1994).
[19] W. Chen, M. Schröder, R. M. D'Souza, D. Sornette, and J. Nagler, Phys. Rev. Lett. **112**, 155701 (2014).
[20] J. Meng, J. Fan, Y. Ashkenazy, and S. Havlin, Chaos **27**, 035807 (2017).
[21] O. C. Guez, A. Gozolchiani, and S. Havlin, Phys. Rev. E **90**, 062814 (2014).
[22] R. Sonone, R. Saha, and N. Gupte, Ind. Acad. Sci. Conf. Ser. **3**, 143 (2020).
[23] E. Surovyatkina (private communication).